THE JOURNAL OF PHYSICAL CHEMISTRY B

Article

pubs.acs.org/JPCB

Atropisomerism of the Asn α Radicals Revealed by Ramachandran Surface Topology

Klára Z. Gerlei,[†] Imre Jákli,[‡,§] Milán Szőri,[†] Svend J. Knak Jensen,[∥] Béla Viskolcz,[†] Imre G. Csizmadia,[†,§,⊥] and András Perczel*[,‡,§,▽]

[†]Department of Chemical Informatics, Faculty of Education, University of Szeged, 6726 Szeged, Hungary

[‡]Protein Modeling Group HAS-ELTE, Institute of Chemistry, Eötvös Loránd University, Pázmány Péter sétány 1/A, H-1117 Budapest, Hungary

[§]Open Laboratory of Protein Science, Institute of Chemistry, Eötvös Loránd University, Pázmány Péter sétány 1/A, H-1117 Budapest, Hungary

[∥]Department of Chemistry, Langelandsgade 140, University of Aarhus, DK-8000 Aarhus C, Denmark

[⊥]Department of Chemistry, University of Toronto, Toronto, Ontario, Canada M5S 3H6

[▽]Laboratory of Structural Chemistry and Biology, Institute of Chemistry, Eötvös Loránd University, Pázmány Péter sétány 1/A, H-1117 Budapest, Hungary

Supporting Information

ABSTRACT: C radicals are typically trigonal planar and thus achiral, regardless of whether they originate from a chiral or an achiral C-atom (e.g., C−H + •OH → C• + H_2O). **Oxidative stress** could initiate radical formation in proteins when, for example, the H-atom is abstracted from the Cα-carbon of an amino acid residue. Electronic structure calculations show that such a radical remains achiral when formed from the achiral Gly, or the chiral but small Ala residues. However, when longer side-chain containing proteogenic amino acid residues are studied (e.g., Asn), they provide radicals of axis chirality, which in turn leads to **atropisomerism** observed for the first time for peptides. The two **enantiomeric** extended backbone **structures**, $\bullet\beta_L$ and $\bullet\beta_D$, interconvert via a pair of **enantiotopic reaction paths**, monitored on a 4D Ramachandran surface, with two distinct transition states of very different *Gibbs*-free energies: 37.4 and 67.7 kJ/mol, respectively. This discovery requires the reassessment of our understanding on radical formation and their conformational and stereochemical behavior. Furthermore, the atropisomerism of proteogenic amino acid residues should affect our understanding on radicals in biological systems and, thus, reframes the role of the D-residues as markers of **molecular aging**.

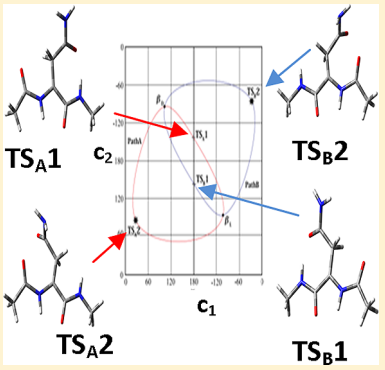

INTRODUCTION

It has been discovered recently that, despite the belief that living cells are solely composed of L-α-amino acids, D-residues also occur in human tissues. Furthermore, the percentage of D-amino acid residues increases with aging of the organism.[1] The role of free radicals in biological systems has been recognized both in essential biochemical reactions[2] and in the destructive oxidative stress.[3] Numerous diseases, such as Alzheimer's, Parkinson's, type II diabetes, vascular dementia,[4−6] as well as aging,[7−9] are attributed to oxidative stress.[10−17] To understand the molecular basis of such diseases, it is essential to characterize the associated free radicals, their stereochemical behavior, arising from the interaction of reactive oxygen species ($O_2^{-\bullet}$, H_2O_2, and HO•) with proteogenic amino acid residues.[18,19]

In general, atropisomerism is a manifestation of conformational changes, as shown in Scheme 1. The clockwise (P or +) and the counter-clockwise (M or −) torsion amounts to axis chirality. In the case of symmetric molecular structures (like X−

Scheme 1. Definition for Atropisomerism in Symmetric Molecular Structures as Non-Superimposable Mirror Images

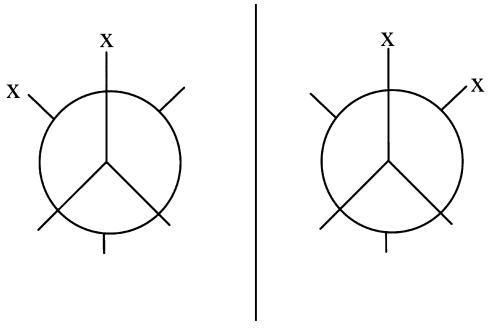

Received: July 17, 2013
Revised: September 7, 2013
Published: September 9, 2013

Scheme 2. L to D Enantiomerization of Asn *via* α-Free-Radical Formation

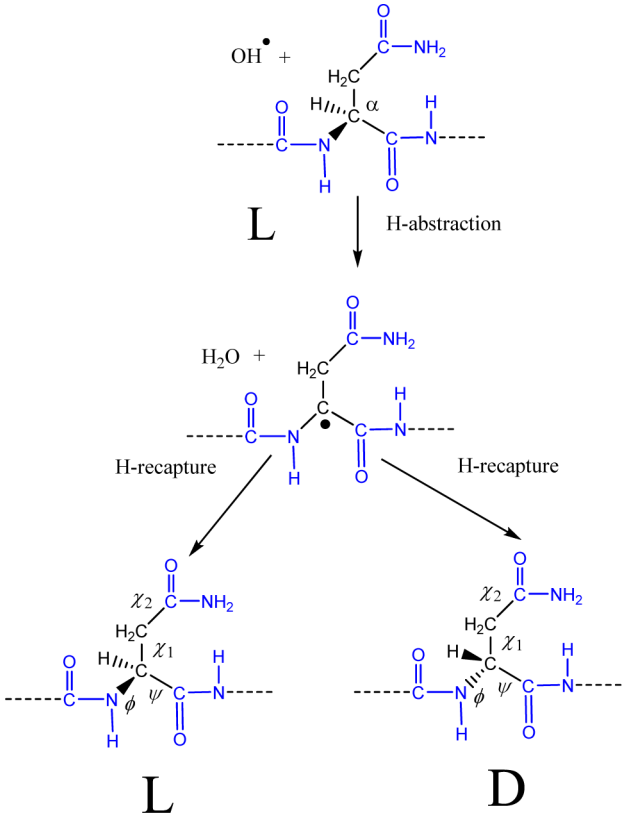

Y−Y−X), the g^+ and g^- conformers are in enantiomeric relationships.

Electronic structure calculations were carried out on small achiral and chiral α-L-amino acid residues[18] such as glycine and alanine diamides. As expected both for Gly and Ala, the alpha radicals formed are achiral and planar. However, for the remaining 17 natural amino acid residues, it was unclear whether, due to side-chain conformation induced structure stabilization, the emerging Cα radicals also remain achiral. In order to answer this question, we have chosen asparagine (Asn) diamide, equipped with a short but polar side chain, to elaborate the chirality properties of the rising Cα radicals both for L- and D-Asn. Note that the short polar side chain of Asn contains an amide group as peptides and proteins backbone do, which could be involved in stabilizing alternatively the Cα radicals via side-chain to backbone H-bond(s). Asparagine is a key amino acid residue of mammalian cells, playing an important role in the biosynthesis of glycoproteins,[20−22] often present in the active sites of various enzymes.[23,24]

Our present aim is to determine whether the Cα radical of Asn is chiral or achiral! If the radical turns out to be chiral, then the L to D enantiomerization phenomena would have far-reaching consequences (Scheme 2).

SCOPE

The achiral nature of the planar Cα radicals both for Gly[18] and Ala[25] derivatives has already been demonstrated. For Ala, the orientation of the C3 symmetric methyl group leads to no alteration of the molecular structure. Thus, the planar radicals derived either from the L- or D-stereoisomers become identical. The conformational properties of both could be depicted by using the very same 2D *Ramachandran* potential energy surface (PES):

Scheme 3. Structures of the Enantiomeric L- and D-Asn Diamides in Their Extended Backbone Conformers, Namely, β_L and β_D

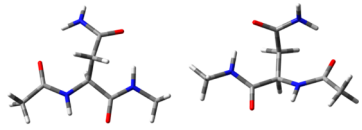

L-Asn diamide D-Asn diamide

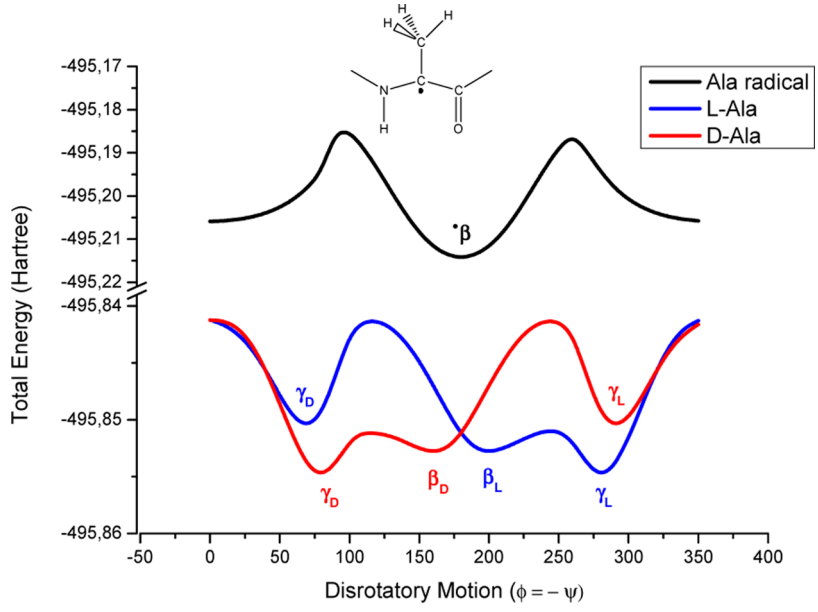

Figure 1. Potential energy curves along the disrotatory ($\phi = -\psi$) cross section of the 2D Ramachandran potential energy surface, $E = f(\phi, \psi)$, for N- and C-protected Ala enantiomeric pairs (in color) and their "common" achiral α radical (in black).

dx.doi.org/10.1021/jp4070906 | J. Phys. Chem. B 2013, 117, 12402−12409

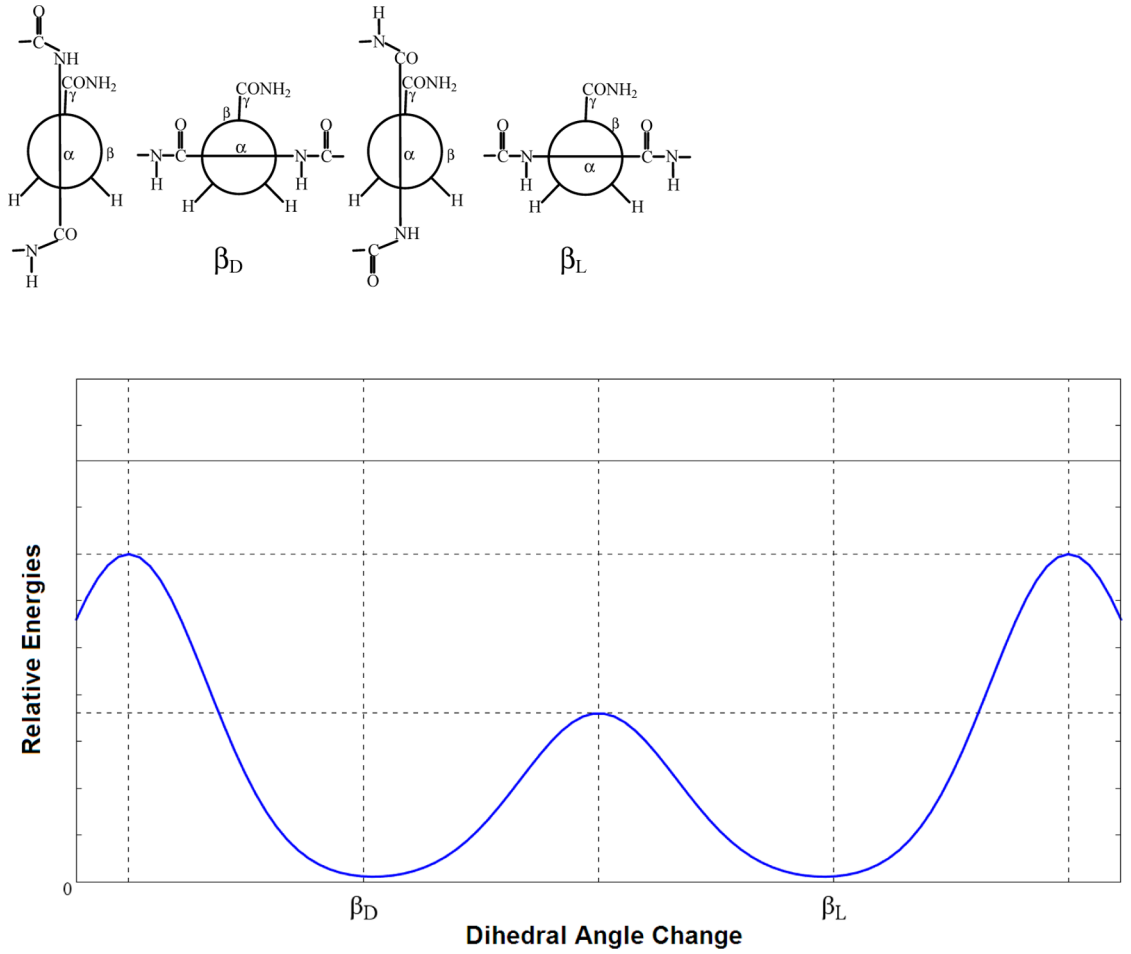

Figure 2. Schematic energy profile of Asn •β_D and •Asn β_L radicals.

$$E = f(\phi, \psi) \tag{1}$$

This different behavior is illustrated by the disrotatory ($\phi = -\psi$) cross section of the three PESs (shown as three potential energy curves, PECs). Figure 1 shows that the PECs of the L- and D-Ala are non-superimposable mirror images. Therefore, for the radical formed from either L- or D-Ala, only a common PEC can be assigned, and thus, only a single radical conformation does exist, which is planar and achiral!

However, compared to Ala, any amino acid residue with a longer and more complex side-chain might behave differently, as exemplified by Asn (Scheme 3).

When Hα atoms are removed from Asn, the resultant Cα radicals become either planar or quasi planar for both isomers. However, the side-chain orientations will be different in the •Asn β_L and the •Asn β_D conformers. The two radicals are non-superimposable mirror image structures due to the axis chirality about χ_1 and χ_2. However, the two backbone structures are interconvertible by rotation about their dihedral angles. (Figure 2 shows schematically what might be expected in such a conformational interconversion.) The difference between the two barrier heights is expected to be different, due to the different magnitude in interaction between the eclipsed groups. In connection with atropisomerism, such a difference was first noticed in the internal rotational potentials of certain biphenyls.[26−28]

RESULTS AND DISCUSSION

Conformational properties of an Asn diamide can only be provided by using the full 4D Ramachandran hypersurface (PEHS):

$$E = f(\phi, \psi, \chi_1, \chi_2) \tag{2}$$

The same holds for the Cα radical of Asn diamide. However, a convenient way to represent the 4D Ramachandran surface is by 2D cross sections of the parent 4D PEHS. Such 2D PESs may be generated, one for the backbone (BB) and one for the side chain (SC):

$$E_{BB} = f(\phi, \psi) \tag{3}$$

$$E_{SC} = f(\chi_1, \chi_2) \tag{4}$$

These 2D cross sections are shown in Figure 3. The top two PES(ϕ, ψ) cross sections were generated with fixed χ_2 and relaxed χ_1. The variation in χ_1 slightly influenced the shape of the two surfaces, but the differences that occurred are hardly visible. In contrast to this, the bottom two PES(χ_1, χ_2) cross sections were generated with relaxed ϕ and ψ values. Since these ϕ, ψ dihedral angles were close to the deepest global minimum, they hardly change and remained in the vicinity of 180°. Consequently, the bottom two PESs look virtually identical.

The backbone 2D cross sections are also shown for D- and L-Asn diamides as well as their alpha radicals in Figure 4 in their

dx.doi.org/10.1021/jp4070906 | J. Phys. Chem. B 2013, 117, 12402−12409

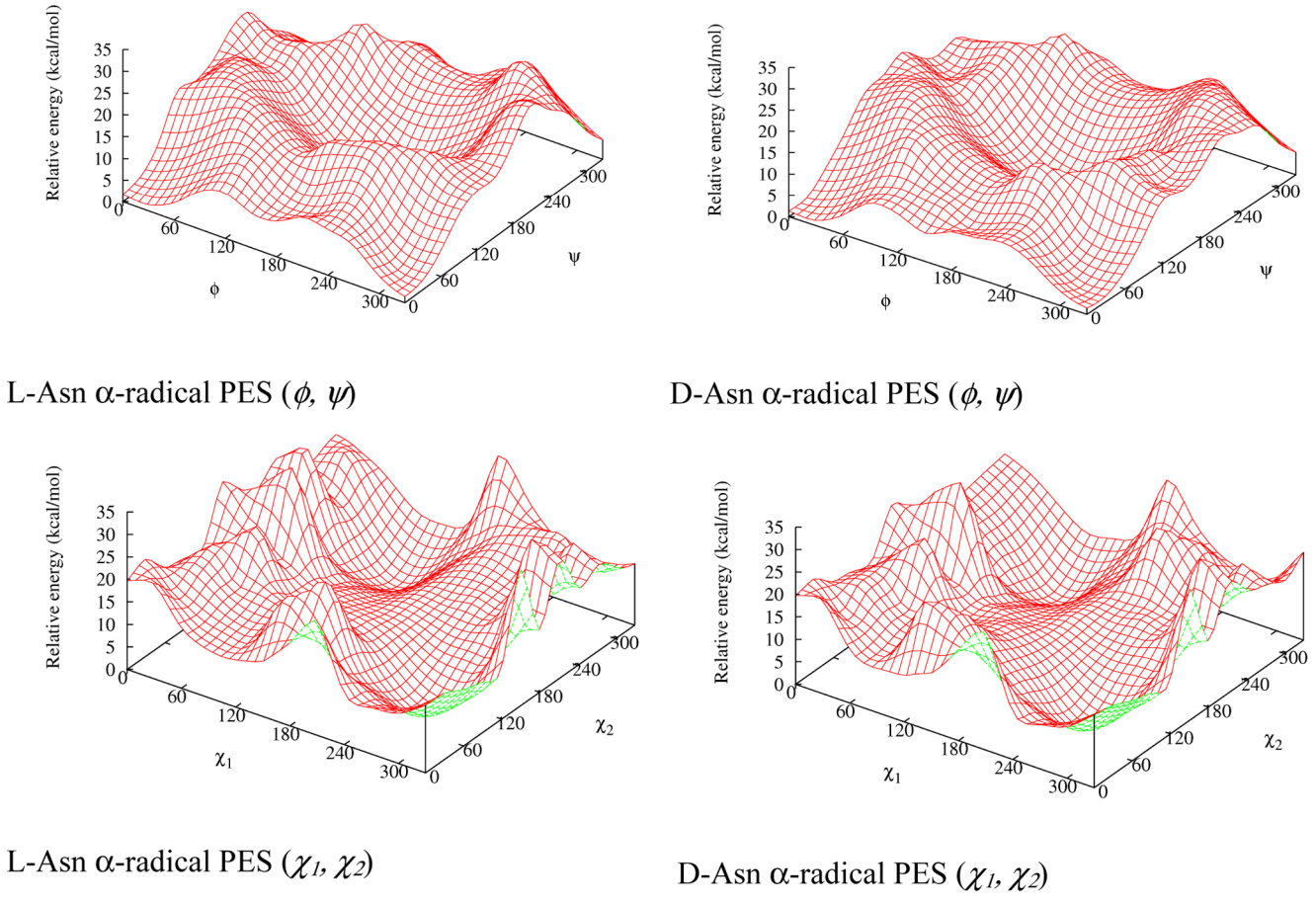

Figure 3. 2D cross sections of the 4D Ramachandran map for the backbone (ϕ, ψ) and the side chain (χ_1, χ_2) of dihedral angles of Cα radicals, which were generated from L- and D-Asn diamides, respectively.

toroidal representations.[29] These toroidal images of the 2D PES are two non-superimposable mirror images of the L- and D-Asn diamides. However, the two radical toroids are identical, suggesting that the two radical enantiomers are located on the same 2D PES.

So far, we may conclude that each of the two parent amino acids, D-Asn and L-Asn, may be represented by a pair of 4D Ramachandran maps, as specified by eq 2. This pair of 4D Ramachandran PEHSs is non-superimposable mirror images of each other, due to their chirality. In contrast to that, when alpha radicals are formed from these enantiomeric pairs, a single 4D PEHS will represent the two Cα radicals (Figures 3 and 4). Such a single PEHS, representing the Cα radical will have two enantiomeric minima corresponding to the $\bullet\beta_L$ and $\bullet\beta_D$ Cα radicals that are non-superimposable mirror images. Nevertheless, they are rotamers or foldamers associated with their single 4D PEHS.

We shall concentrate on the analysis on this 4D Ramachandran PEHS of the Cα radical obtained from the two enantiomeric pairs of Asn. Two geometrically extended radicals were obtained, which are denoted as $\bullet\beta_D$ and $\bullet\beta_L$ (Figure 4). The optimized dihedral angles and the stability of both $\bullet\beta_D$ and $\bullet\beta_L$ radicals are given in the first two lines in Table 1. The careful search on the 4D PEHS (eq 2) associated with these radicals revealed four transition states which correspond to two pairs, denoted by A and B. Each of these two pairs had a high and a low transition state, as shown in the last four lines in Table 1.

Conformational changes, with such low activation energies as 40 and 74 kJ/mol, could occur at body temperature; therefore, topomerization is possible before amino acid racemization by H-abstraction takes place.

The magnitudes and signs of the optimized dihedral angles reveal that the A- and B-paths are enantiotopic ones.[30] These are depicted schematically on the backbone (eq 3) and side chain (eq 4) to the 2D cross sections in Figure 5.

This figure indicates that there are two paths labeled A and B of the enantiomeric topomerization in which ϕ and ψ are changing to a considerably smaller extent than χ_1 and χ_2 in the conversion between $\bullet\beta_L$ and $\bullet\beta_D$ minima. Of the four transition states, TS_A1 and TS_A2 are associated with path A, while TS_B1 and TS_B2 are connected to path B.

The energy profiles of the A and B paths are shown in the top portion of Figure 6, where TS1 corresponds to the lower transition state and TS2 corresponds to the higher transition state. Since the two paths are enantiotopic, it seems reasonable to assume that one of them corresponds to clockwise and the other one corresponds to counterclockwise motion. If we draw the potential energy curve on a surface of a cylinder, then indeed we have only two transition states TS1 and TS2 and path A and path B correspond to clockwise and counterclockwise motions along the potential energy curve.

A linear cross section was generated to show structures ($\bullet\beta_L$ and $\bullet\beta_D$) as depicted in Figure 7 and Table 2. This result is in agreement with the conclusion that the 4D Ramachandran PEHS of the α radical of Asn diamide contains the

dx.doi.org/10.1021/jp4070906 | J. Phys. Chem. B 2013, 117, 12402−12409

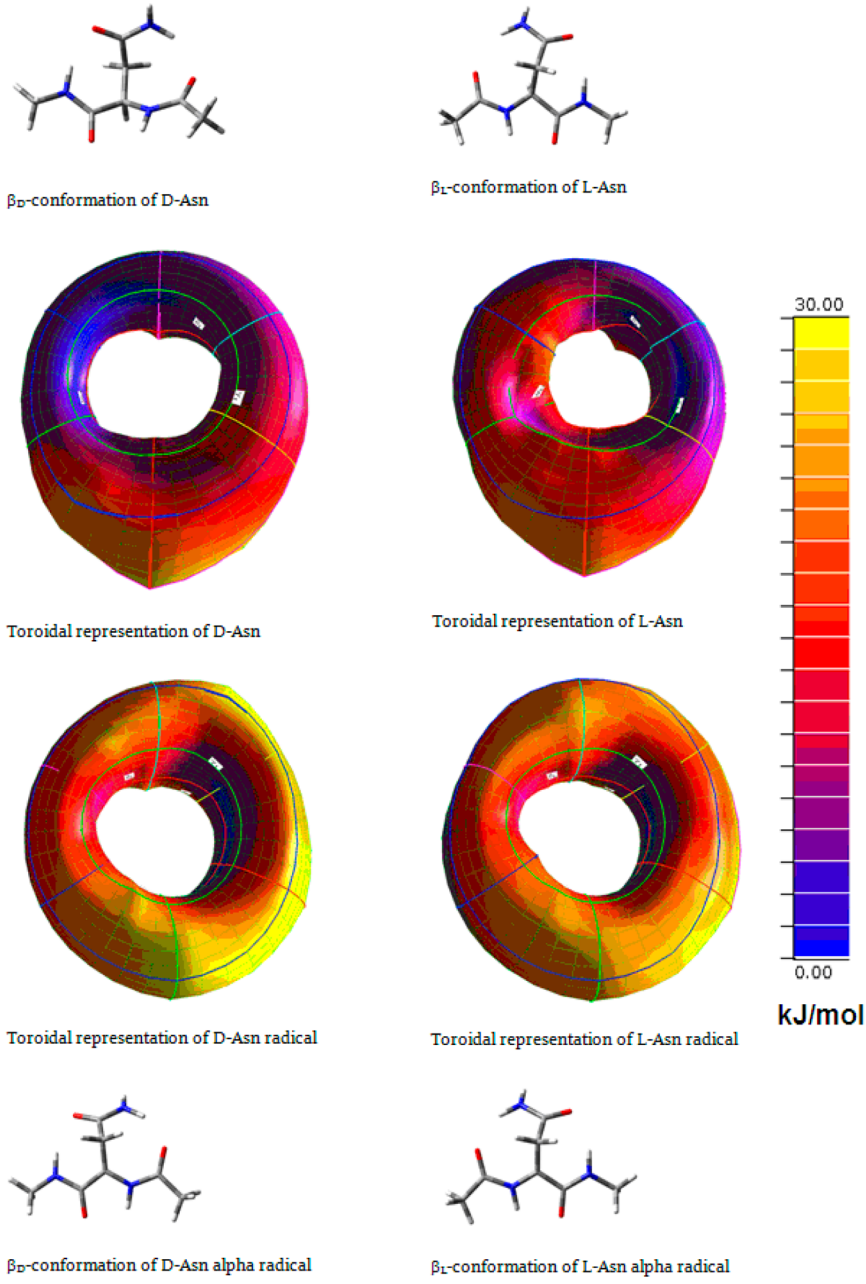

Figure 4. Top: D- and L-Asn diamide structure and 2D Ramachandran toroidal representation. Bottom: D-L-Asn Cα radical structure and toroidal representation of the 2D Ramachandran PES. The dihedral angles, taken from the B3LYP/6-31G* calculations, indicate the mirror image structures of the enantiomeric pairs. The step size of the color scale in this figure is 1.5 kJ/mol.

Table 1. Structure and Stability of $\bullet\beta_L$ and $\bullet\beta_D$ C-α Radicals of Asn Diamide and Their Interconnecting Transition States[a]

CP[b]	ω_0	ϕ	ψ	ω	χ_1	χ_2	ΔE[c]
$\beta_L\bullet$	−177.27	−165.66	171.72	−176.11	−103.37	93.94	0.00
$\beta_D\bullet$	177.21	165.68	−171.71	176.09	103.35	−93.93	0.00
TS_A1	180.00	−178.01	175.84	−176.91	179.06	−143.32	40.29
TS_A2	179.00	158.75	174.06	−176.21	27.32	86.22	74.97
TS_B1	−179.82	178.55	−176.00	176.92	−179.43	143.45	40.28
TS_B2	−178.94	−158.51	−174.01	176.35	−28.04	−85.67	74.93

[a]Optimized at the B3LYP/6-31G(d) level of theory: β_L = −663.926192 in hartree. [b]Critical points. [c]In kJ/mol.

enantiomeric radicals ($\bullet\beta_L$ and $\bullet\beta_D$) that are interrelated by axis chirality; therefore, they are conformationally convertible.

In order to assess the accuracy of Gibbs free energy change, geometry optimizations were repeated at the B3LYP/6-311+G(d,p) level of theory. These optimizations were augmented by single point coupled cluster (CCSD(T)) calculations. The DFT ΔG^0 values are shown in comparison to MP2 and CCSD(T) results in Table 3.

dx.doi.org/10.1021/jp4070906 | J. Phys. Chem. B 2013, 117, 12402−12409

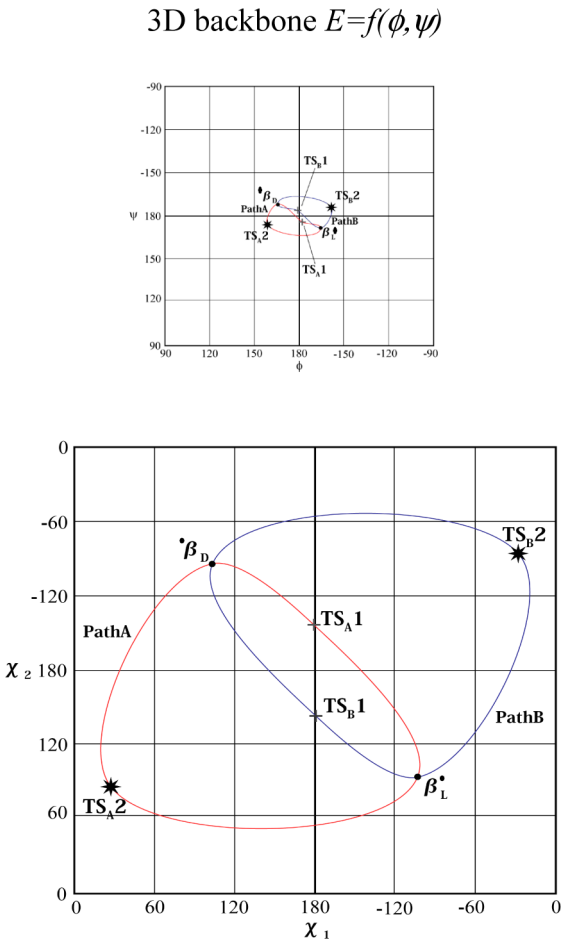

Figure 5. Schematic illustration of enantiomeric topomerization paths A and B on the 2D PES cross sections associated with backbone (top) and side-chain (bottom) conformational change.

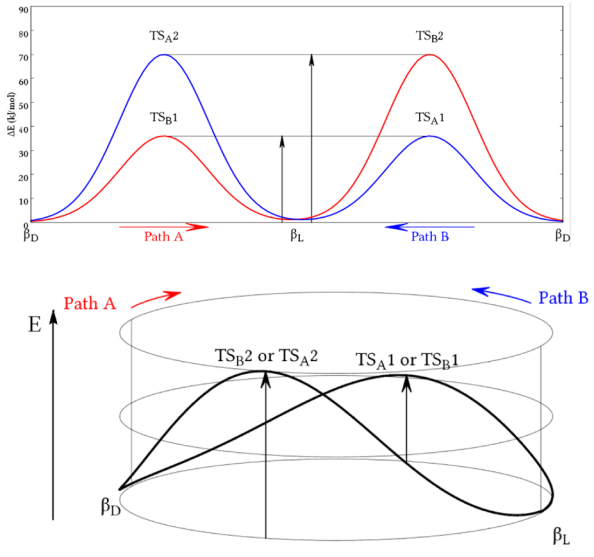

Figure 6. Energy profiles for enantiotopic topomerization along paths A and B, on the 4D Ramachandran type potential energy hypersurface PEHS, of L- and D-Asn diamide Cα radicals in their extended (β) conformations.

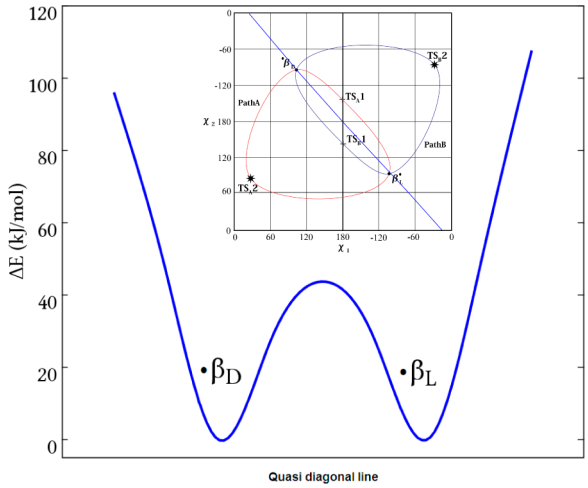

Figure 7. Quasi diagonal cross section of the 4D Ramachandran PEHS of the Cα radical of Asn diamide. Relative positions are with respect to the 180−180 central point.

Table 2. Dihedral Angles and Relative Energies (kJ/mol) for the Quasi Diagonal Cross Sections[a]

relative position	ϕ	ψ	χ_1	χ_2	energy
4.00	−151.3	163.4	−26.7	7.9	−663.89
3.00	−158.5	167.6	−65.1	50.9	−663.91
2.00	−165.7	171.7	−103.4	93.9	−663.93
1.00	−172.8	175.9	−141.7	137	−663.92
0.00	−180	−180	180	180	−663.91
−1.00	172.8	−175.9	141.7	−137	−663.92
−2.00	165.7	−171.7	103.4	−93.9	−663.93
−3.00	158.5	−167.6	65	−50.9	−663.91
−4.00	151.4	−163.4	26.7	−7.9	−663.89

[a]Energy values are given in kJ/mol, β_L = −663.926192 in hartree.

Both radicals can be converted to D- and L-asparagine by hydrogen abstraction. Even if both •β_L and •β_D may be converted nearly in 50:50 ratio to D- and L-Asn diamide, nevertheless the D amino acid concentration will be on the rise, since the biological system has started with 100% pure L-Asn diamide.

CONCLUSIONS

It has been demonstrated that each of the D- and L-Asn peptide model conformations can be represented by a 4D Ramachandran potential energy surface, which are mathematical objects of non-superimposable mirror image structures. In contrast to this, the Cα radical, generated from the two enantiomeric D- and L-Asn diamides, can be represented by a single 4D Ramacahandran PES, which has a pair of enantiomeric free radicals of extended configurations, denoted by •β_L and •β_D. These non-superimposable enantiomers are atropisomers due to axis chirality of the side-chain dihedral angles! The topology of this 4D Ramachandran PES revealed epimeric topomerization paths with a pair of transition states where the lower one was in the range of 32−36 kJ/mol and the higher one in the range of 65−68 kJ/mol, respectively. By hydrogen atom abstraction, both •β_L and •β_D radicals can be converted to L- and D-Asn, thereby increasing the D-amino acid content of the human body. Such a mechanism could produce an increasing amount of D-amino acids coupled to the aging process.[1]

dx.doi.org/10.1021/jp4070906 | J. Phys. Chem. B 2013, 117, 12402−12409

Table 3. Free Energy Changes, ΔG^0 (kJ/mol), of Radical Formation and Enantiomeric Topomerization Computed at Several Levels of Theory

	DFT[a]				MP2[b]			
species	ΔE_1	corr[c]	ΔG_1^{0} [d]	E(CC[e])	ΔE_2	corr[c]	ΔG_2^{0} [d]	E(CC[e])
Asn β_L	−1676.26	31.03	−1645.23	−1604.90	−1694.57	32.22	−1662.35	−1602.40
Asn β_D	−1676.26	31.03	−1645.23	−1604.90	−1694.57	32.22	−1662.35	−1602.40
•Asn β_L	0.00	0.00	0.00	0.00	0.00	0.00	0.00	0.00
•Asn β_D	0.00	0.00	0.00	0.00	0.00	0.00	0.00	0.00
TS A1	38.47	−5.90	32.57	43.29	42.71	−7.34	35.37	42.29
TS B1	38.47	−5.88	32.58	43.28	42.71	−7.34	35.38	42.29
TS A2	70.88	−5.46	65.42	67.50	72.80	−5.11	67.69	63.72
TS B2	70.87	−5.46	65.41	67.49	72.80	−5.11	67.69	63.72

[a]Geometry optimized at the B3LYp/6-311++G(d,p) level of theory (calculated vibrational wavenumbers are scaled by 0.97). [b]Values are obtained by the MP2/cc-pVTZ//B3LYp/6-311++G(d,p) level of theory. [c]Correction for ΔE to ΔG^0. [d]For dissociation free energy, ΔG^0 must be reduced by the hydrogen energy, which may take 0.5 hartree (1312.75 kJ/mol). [e]Values are obtained by the CCSD(T)/cc-pVTZ//B3LYp/6-311++G(d,p) level of theory.

However, if the barrier for g− → g+ interconversion is very high, then the two conformers become isolable even at room temperature, and thus atropisomers are obtained. Axis chirality is a dominant factor in biologically important molecules and plays a noticeable role in peptide and protein folding. Here we have shown how atropisomers can "self" stabilize for a Cα radical of an amino acid residue. However, the present finding could hold for several proteogenic residues, except Gly and Ala.

Research is now in progress in studying Asp acid diamide. The preliminary results already indicate that the radical of Asp radical behaves similarly to that of Asn.

METHODS

Preliminary geometry optimization was completed at the B3LYP/6-31G(d) level of theory, reoptimized at the B3LYP/6-311++G(d,p) level of theory. Gibbs free energies were determined at the MP2/cc-pVTZ and CCSD(T)/cc-pVTZ levels of theory by using B3LYP/6-311++G(d,p) geometries.

ASSOCIATED CONTENT

Supporting Information

Z-matrices of the calculated structures. Copy of the original publication of the first Gaussian HF-MO molecular computation. This material is available free of charge via the Internet at http://pubs.acs.org.

AUTHOR INFORMATION

Corresponding Author

*E-mail: perczel@chem.elte.hu. Phone: +36-1-272-2500/1653.

Notes

The authors declare no competing financial interest.

ACKNOWLEDGMENTS

This paper commemorates the 50th anniversary of the first *ab initio* Gaussian MO computation carried out on an organic molecule, HCOF, at MIT (cf. the Supporting Information). We thank László Müller and Máté Labádi for the administration of the computing system used for this work. We also thank Gábor Sallai for his help. This work was supported by TAMOP4.2.1/B-09-1/KNOV-210-0005 and the Hungarian Scientific Research Fund (OTKA K72973, NK101072) and TÁMOP-4.2.1.B-09/1/KMR.

REFERENCES

(1) Fujii, N. D-Amino Acid Biosystem. *Biol. Pharm. Bull.* **2005**, *28*, 1585−1589.

(2) Kobliakov, V. A. Mechanisms of Tumor Promotion by Reactive Oxygen Species. *Biochemistry (Moscow)* **2010**, *75*, 675−685.

(3) Stadtman, E. R. Protein Oxidation and Aging. *Free Radical Res.* **2006**, *40*, 1250−1258.

(4) Cohen, S. M. Promotion in Urinary Bladder Carcinogenesis. *Environ. Health Perspect.* **1983**, *50*, 51−59.

(5) Rauk, A. The Chemistry of Alzheimer's Disease. *Chem. Soc. Rev.* **2009**, *38*, 2698−2715.

(6) Han, W.; Li, C. Linking Type 2 Diabetes and Alzheimer's Disease. *Proc. Natl. Acad. Sci. U.S.A.* **2010**, *107*, 6557.

(7) Fatehi-Hassanabad, Z.; Chan, C. B.; Furman, B. L. Reactive Oxygen Species and Endothelial Function in Diabetes. *Eur. J. Pharmacol.* **2010**, *636*, 8−17.

(8) Jenner, P. Oxidative Stress in Parkinson's Disease. *Ann. Neurol.* **2003**, *53*, S26−S36.

(9) Bamham, K. J.; Masters, C. L.; Bush, A. I. Neurodegenerative Diseases and Oxidative Stress. *Nat. Rev. Drug Discovery* **2004**, *3*, 205−214.

(10) Serra, J. a; Domínguez, R. O.; Marschoff, E. R.; Guareschi, E. M.; Famulari, A. L.; Boveris, A. Systemic Oxidative Stress Associated with the Neurological Diseases of Aging. *Neurochem. Res.* **2009**, *34*, 2122−32.

(11) Robinson, N. E.; Robinson, a B. Molecular Clocks. *Proc. Natl. Acad. Sci. U.S.A.* **2001**, *98*, 944−9.

(12) Agha-Hosseini, F.; Mirzaii-Dizgah, I.; Farmanbar, N.; Abdollahi, M. Oxidative Stress Status and DNA Damage in Saliva of Human Subjects with Oral Lichen Planus and Oral Squamous Cell Carcinoma. *J. Oral Pathol. Med.* **2012**, *41*, 736−40.

(13) Ohta, M.; Higashi, Y.; Yawata, T.; Kitahara, M.; Nobumoto, A.; Ishida, E.; Tsuda, M.; Fujimoto, Y.; Shimizu, K. Attenuation of Axonal Injury and Oxidative Stress by Edaravone Protects Against Cognitive Impairments After Traumatic Brain Injury. *Brain Res.* **2013**, *1490*, 184−92.

(14) Gu, X.; Sun, J.; Li, S.; Wu, X.; Li, L. Oxidative Stress Induces DNA Demethylation and Histone Acetylation in SH-SY5Y Cells: Potential Epigenetic Mechanisms in Gene Transcription in Aβ Production. *Neurobiol. Aging* **2013**, *34*, 1069−79.

(15) Chuang, H.-C.; Hsueh, T.-W.; Chang, C.-C.; Hwang, J.-S.; Chuang, K.-J.; Yan, Y.-H.; Cheng, T.-J. Nickel-Regulated Heart Rate Variability: The Roles of Oxidative Stress and Inflammation. *Toxicol. Appl. Pharmacol.* **2013**, *266*, 298−306.

(16) Flores, L. C.; Ortiz, M.; Dube, S.; Hubbard, G. B.; Lee, S.; Salmon, A.; Zhang, Y.; Ikeno, Y. Thioredoxin, Oxidative Stress, Cancer and Aging. *Longevity Healthspan* **2012**, *1*, 4.

(17) Kotsinas, A.; Aggarwal, V.; Tan, E.-J.; Levy, B.; Gorgoulis, V. G. PIG3: A Novel Link Between Oxidative Stress and DNA Damage Response in Cancer. *Cancer Lett.* **2012**, *327*, 97−102.
(18) Owen, M. C.; Szori, M.; Csizmadia, I. G.; Viskolcz, B. Conformation-Dependent •OH/H2O2 Hydrogen Abstraction Reaction Cycles of Gly and Ala Residues: a Comparative Theoretical Study. *J. Phys. Chem. B* **2012**, *116*, 1143−54.
(19) Galano, A.; Alvarez-Idaboy, J.; Bravo-Pérez, G.; Ruiz-Santoyo, M. E. Mechanism and Rate Coefficients of the Gas Phase OH Hydrogen Abstraction Reaction from Asparagine: a Quantum Mechanical Approach. *J. Mol. Struct.: THEOCHEM* **2002**, *617*, 77−86.
(20) O'Connor, S. E.; Imperiali, B. Conformational Switching by Asparagine-Linked Glycosylation. *J. Am. Chem. Soc.* **1997**, *119*, 2295−2296.
(21) Imperiali, B.; Shannon, K.; Rickert, K. Role of Peptide Conformation in Asparagine-Linked Glycosylation. *J. Am. Chem. Soc.* **1992**, *114*, 7942−7944.
(22) Imperiali, B. Protein Glycosylation: The Clash of the Titans. *Acc. Chem. Res.* **1997**, *30*, 452−459.
(23) Mansfeld, J.; Gebauer, S.; Dathe, K.; Ulbrich-Hofmann, R. Secretory Phospholipase A2 from Arabidopsis Thaliana: Insights into the Three-Dimensional Structure and the Amino Acids Involved in Catalysis. *Biochemistry* **2006**, *45*, 5687−5694.
(24) Himo, F. Quantum Chemical Modeling of Enzyme Active Sites and Reaction Mechanisms. *Theor. Chem. Acc.* **2005**, *116*, 232−240.
(25) Owen, M. C.; Viskolcz, B.; Csizmadia, I. G. Quantum Chemical Analysis of the Unfolding of a Penta-Alanyl 3_{10}-Helix Initiated by $HO^{\bullet}$, $HO_2^{\bullet}$, and $O_2^{-\bullet}$. *J. Phys. Chem. B* **2011**, *115*, 8014−8023.
(26) Tang, T.-H.; Nowakowska, M.; Guillet, J. E.; Csizmadia, I. G. Rotational Barriers for Selected Polyfluorobiphenyl (PFB), Polychlorobiphenyl (PCB) and Polybromobiphenyl (PBB) Congeners. *J. Mol. Struct.* **1991**, *232*, 133−146.
(27) Von Kuhn, R.; Albrecht, O. Über die Racemisierung Optisch Aktiver Diphensauren and über die Schwingungen der Benzolkerne im Diphenylsystem. *Justus Liebigs Ann. Chem.* **1927**, *455*, 272−299.
(28) Christie, G. H.; Kenner, J. H. First Discovered in 2,2′-dinitro-6,6′ -dicarboxylic acid-biphenyl. *J. Am. Chem. Soc.* **1922**, *121*, 614−620.
(29) Jákli, I.; Jensen, S. K.; Csizmadia, I. G.; Perczel, A. Variation of Conformational Properties at a Glance . True Graphical Visualization of the Ramachandran Surface Topology as a Periodic Potential Energy Surface. *Chem. Phys. Lett.* **2012**, *547*, 82−88.
(30) Wolfe, S.; Schlegel, H. B.; Csizmadia, I. G. Bernardi The Chemical Dynamics of Symmetric and Asymmetric Reaction Coordinates. *J. Am. Chem. Soc.* **1975**, *97*, 2020−2024.